A&A 488, 1007–1015 (2008)
DOI: 10.1051/0004-6361:200809930

Astronomy & Astrophysics

Evolution of stellar collision products in open clusters

I. Blue stragglers in N-body models of M 67

E. Glebbeek[1], O. R. Pols[1], and J. R. Hurley[2]

[1] Sterrekundig Instituut Utrecht, Postbus 80000, 3508 TA Utrecht, The Netherlands
e-mail: e.glebbeek@astro.uu.nl
[2] Centre for Astrophysics and Supercomputing, Swinburne University of Technology, Hawthorn VIC 3122, Australia

Received 8 April 2008 / Accepted 4 June 2008

ABSTRACT

Stellar collisions are an important formation channel for blue straggler stars in globular and old open clusters. Hydrodynamical simulations have shown that the remnants of such collisions are out of thermal equilibrium, are not strongly mixed and can rotate very rapidly. Detailed evolution models of collision products are needed to interpret observed blue straggler populations and to use them to probe the dynamical history of a star cluster. We expand on previous studies by presenting an efficient procedure to import the results of detailed collision simulations into a fully implicit stellar evolution code. Our code is able to evolve stellar collision products in a fairly robust manner and allows for a systematic study of their evolution.
Using our code we have constructed detailed models of the collisional blue stragglers produced in the *N*-body simulation of M 67 performed by Hurley et al. in 2005. We assume the collisions are head-on and thus ignore the effects of rotation in this paper. Our detailed models are more luminous than normal stars of the same mass and in the same stage of evolution, but cooler than homogeneously mixed versions of the collision products. The increased luminosity and inefficient mixing decrease the remaining main-sequence lifetimes of the collision products, which are much shorter than predicted by the simple prescription commonly used in *N*-body simulations.

Key words. stars: formation – stars: blue stragglers – Galaxy: open clusters and associations: general – methods: numerical – stars: evolution – stellar dynamics

1. Introduction

Blue stragglers are stars that appear above and blueward of the main sequence turnoff in the colour-magnitude diagrams (CMDs) of star clusters, with masses larger than that of a turnoff star. They were first identified by Sandage (1953) in the globular cluster M 3 and soon afterwards in the old open cluster M 67 (Johnson & Sandage 1955). Blue stragglers have since been found in other globular clusters and in open clusters of all ages (Ahumada & Lapasset 1995). Various mechanisms have been proposed for their formation (Stryker 1993). Currently, there are three accepted formation channels: mass transfer due to Roche-lobe overflow in binary systems, and stellar mergers, either due to dynamical collisions or through coalescence of close binaries.

Hills & Day (1976) first showed that physical collisions between main-sequence stars are likely to occur in the dense cores of some globular clusters. In most environments collisions between single stars are very rare, but binary systems can significantly enhance the rate of stellar collisions because of their much larger collisional cross sections. Stellar collisions are thus an important formation channel for blue stragglers even in old open clusters such as M 67, as is demonstrated by direct *N*-body calculations (Hurley et al. 2001, 2005). These simulations indicate that, while all the above-mentioned formation mechanisms operate in different regions of the cluster and all are needed to reproduce the observed blue straggler population, all formation paths – including binary mass transfer and binary coalescence – are strongly affected by the dynamical evolution of the cluster. The blue straggler population therefore contains important information on the dynamical history of a cluster. Extracting this information requires understanding not only how blue stragglers are formed but also how they subsequently evolve.

In *N*-body models collisions between two main-sequence stars are usually approximated by assuming that the stars merge without mass loss and replacing the end product by a normal (evolved) main-sequence star with its age reset in accordance with the assumption of complete mixing (Tout et al. 1997; Hurley et al. 2002). Smoothed particle hydrodynamics (SPH) simulations of stellar mergers (Lombardi et al. 1995, 1996) show that some mass is lost during the collision and that the collision products are generally far from being fully mixed. To understand how this affects their further evolution and the predicted blue straggler population, detailed stellar evolution models of the collision products are needed.

In early attempts to model the evolution of stellar merger remnants simplifying assumptions were made: the two stars were assumed to mix completely (Bailyn & Pinsonneault 1995), a specified chemical profile was imposed on the remnant (Sills et al. 1995) or a simplified prescription for heating during the collision was applied to mimic the presumed pre-main sequence contraction phase of evolution (Sandquist et al. 1997). The first realistic evolution calculations of collision products were performed by Sills et al. (1997) who took SPH simulations of head-on collisions between detailed stellar models and imported the SPH results into a stellar evolution code. Their models demonstrated that none of the previously made simplifications are

valid: although the collision products are inflated due to shock heating, they do not develop substantial convection zones during thermal relaxation and do not undergo significant mixing during their evolution.

This situation changes when the angular momentum of the collisions is considered. For collisions that are even slightly off-axis, the remnants retain too much angular momentum to relax into thermal equilibrium without reaching break-up velocity (Lombardi et al. 1996). The evolution of such collisions was studied by Sills et al. (2001). In the absence of a clear mechanism by which the stars can lose their excess angular momentum, they artificially removed a large fraction of the angular momentum to allow thermal relaxation. Nevertheless, the remnants continue to rotate rapidly throughout their main-sequence evolution and rotational mixing makes the remnants bluer and brighter and significantly extends their lifetimes. These conclusions were confirmed by higher-resolution calculations (Sills et al. 2002).

The above studies have focussed on blue stragglers in globular clusters, and investigated only a few interesting cases. This limitation was imposed by the computation time required and numerical difficulties in the evolution calculations. However, the importance of stellar collisions for the evolution of star clusters calls for a more systematic approach, covering a larger parameter space and extending to higher masses and younger clusters. This is the aim of our current work. We have developed a flexible evolution code that is able to evolve stellar collision products under a wide range of circumstances in a fairly robust manner. As our code cannot yet treat rotation and rotational mixing properly, for the moment we consider only head-on collisions and ignore the effects of rotation.

As a first step in a systematic study of stellar merger remnants we have constructed detailed models of the blue stragglers formed by stellar collisions in the N-body model of M 67 of Hurley et al. (2005). They evolved a cluster of 36 000 stars from zero age to the age of M 67 (4 Gyr) taking into account both cluster dynamics and stellar and binary evolution. In their simulation the cluster evolution resulted in 20 blue stragglers at 4 Gyr, eight of which had a collisional origin. They formed either as a result of dynamical perturbation of a primordial binary, or as a result of three-body (binary-single star) or four-body (binary-binary) interactions. In two of the latter cases, three stars merged in subsequent collisions with the fourth star ending up as a binary companion to the blue straggler. Hence in total ten collisions were involved in the formation of these eight blue stragglers.

We evolve these collision products with our detailed stellar evolution code and compare these models with the evolution tracks of normal detailed stellar models and fully mixed detailed models, as well as with the parametric models used by Hurley et al. (2005). In particular we investigate the effect on the main-sequence lifetime of the merger product (i.e., the time during which it will be visible as a blue straggler), its position in the Hertzsprung-Russell diagram and the effect on the chemical abundances of the remnant. In a companion paper (Glebbeek & Pols 2008, Paper II) we study the influence of varying the collision parameters, in particular the masses of the two stars and their evolutionary stage.

2. Tools

2.1. Modelling the merging process

To calculate the structure of the collision remnants immediately after the collision we have used the Make Me A Star (MMAS) code developed by Lombardi et al. (2002), which produces a one-dimensional model that approximates the results of detailed smooth particle hydrodynamics (SPH) calculations. The essence of the approximation is the observation that in a stellar model in hydrostatic equilibrium the quantity A defined by

$$A^{3/2} = \frac{(2\pi\hbar^2)^{3/2}}{m_{\rm u}^4}\frac{1}{\mu^4}\prod_i\left[\left(\frac{B_i}{\mu}\right)^{5/2}\frac{\omega_i}{X_i}\right]^{-Y_i} {\rm e}^{S-\frac{5}{2}} \tag{1}$$

increases monotonically from the centre to the surface, at least as long as radiation pressure is negligible (see for instance Lombardi et al. 1996, 2002, for details). Here, S denotes the entropy per particle in units of Boltzmann's constant, μ is the mean molecular weight of the constituent particles, B_i is the mass of particle species i in units of the atomic mass $m_{\rm u}$, X_i and Y_i are their abundance fraction by mass and number, respectively. Note that A is a function of entropy and composition only. The factor ω_i denotes the degeneracy of the ground state and is taken as 1 for nuclei and 2 for electrons. For a classical ideal gas, (1) reduces to

$$A = \frac{P}{\rho^{5/3}} \tag{2}$$

MMAS modifies the initial A profiles of the parent stars to correct for shock heating during the collision and estimates the amount of mass lost. The amounts of shock heating and mass loss are calibrated to detailed SPH results. The remnant profile is then constructed by collecting all mass-bins from the parent stars, sorting them in order of increasing A and integrating the equations of hydrostatic equilibrium and mass conservation.

The composition profile of the remnant is also determined from the A profile. Shock heating leads to partial mixing of adjacent layers in each of the parent stars. After both A individual composition profiles have been corrected for shock heating, the composition in the remnant is set to the average composition of material from the parent stars with that value of A. So if for a particular value of A a fraction f_1 comes from the primary with composition X_1 and a fraction f_2 comes from the secondary with composition X_2, then the composition $X_{\rm r}$ of the corresponding layer in the remnant is

$$X_{\rm r} = X_1 f_1 + X_2 f_2. \tag{3}$$

For more details see Lombardi et al. (2002).

2.2. The stellar evolution code

To calculate the evolution of the parent stars as well as the further evolution of the collision product we use the stellar evolution code (hereafter STARS) originally developed by Eggleton (Eggleton 1971) and updated by others (Pols et al. 1995). The code uses an adaptive non-Lagrangian mesh that allocates meshpoints according to a mesh-spacing function that places more meshpoints in regions where a higher resolution is required. This means that stars can be evolved with reasonable accuracy with as few as 200 meshpoints.

Our version of STARS uses nuclear reaction rates from Caughlan & Fowler (1988) and Caughlan et al. (1985) and opacities from Rogers & Iglesias (1992) and Alexander & Ferguson (1994). The assumed heavy-element composition is scaled to solar abundances (Anders & Grevesse 1989).

STARS is fully implicit and solves the equations for the structure and composition of the star simultaneously. Convection

Table 1. Initial conditions for the collisions and collision product lifetimes. Time is given in millions of years (Myr) and masses are given in solar masses ($M_\odot$). See the main text for a description of the different columns.

ID	t	M_1	M_2	M	$t_{\rm ms}$	$\tau_{\rm ms}$	$\tau_{\rm ms,hom}$	$t_{\rm ms,BSE}$
2203	3480	1.23	0.85	1.93	539	1000	745	991
2321	3960	1.29	0.59	1.74	599	1345	862	1305
2565	3650	0.95	0.94	1.76	1016	1297	1122	1336
2973	3170	0.89	0.80	1.56	1569	1850	1685	1877
3121	3890	1.09	0.54	1.52	1428	1993	1629	2051
3289-1	3610	0.82	0.51	1.25	3157	3736	3736	3910
3289-2	3610		0.76	1.86	1024	1103	1058	1020
3445	2770	0.77	0.76	1.41	2172	2502	2361	2547
3835-1	3797	0.82	0.60	1.32	2657	3090	3090	3191
3835-2	3798		0.31	1.56	1765	1849	1793	1776

is treated using the mixing-length prescription (Böhm-Vitense 1958) and convective mixing is modelled as a diffusion process (Eggleton 1972). We use a ratio of mixing length to local pressure scale height $l/H_{\rm P} = 2.0$.

Usually the mean molecular weight in stars will be either constant in a region or decrease radially outward. In merger remnants there can be layers in which the molecular weight gradient is inverted and a layer of higher mean molecular weight lies on top of a layer of lower mean molecular weight. Such a situation is unstable and leads to a process known as thermohaline mixing (Ulrich 1972; Kippenhahn et al. 1980). The instability arises because material with high molecular weight is supported by thermal buoyancy. When a fluid element exchanges heat with its environment it loses buoyancy and begins to sink on the timescale for heat exchange, i.e. the local thermal timescale. We model this as a diffusion process as described in Stancliffe et al. (2007). The diffusion coefficient is given by the product of the typical velocity and size of the fluid elements and the efficiency of mixing thus depends on their assumed geometry. The efficiency we have adopted in this work corresponds to spherical geometry, as in Kippenhahn et al. (1980). If the fluid blobs are elongated the mixing is more efficient. However, since for our adopted choice the mixing occurs on the local thermal timescale and is fast compared to the nuclear timescale, our results are not sensitive to an increase in the efficiency of thermohaline mixing.

STARS uses a simple model for convective overshooting (Schröder et al. 1997) that allows extra mixing in regions where $\nabla_{\rm rad} - \nabla_{\rm ad} > -\delta$. We have found that this prescription leads to spurious mixing in the cores of some of our collision products (see Sect. 5.1), so we have chosen to disable convective overshooting for this work.

2.3. Constructing starting models for merger remnant evolution

To construct starting models for the collisions we evolved stars of the appropriate masses from the zero-age main sequence (ZAMS) to the time of collision as listed in Table 1 (see Sect. 3). These models were then used as input for MMAS.

The output from MMAS was converted into an input model for STARS using implicit calculations starting from a normal ZAMS model with the same mass as the collision remnant. This model is first evolved until its core hydrogen abundance matches that of the remnant. At this point, the entropy and composition profiles of the model are adjusted to reproduce the profiles of the collision product. Figure 1 shows the profiles at the beginning and end of the iteration as well as the output profiles from MMAS for a generic case. The entropy profile was adjusted by adding an artificial energy source $\epsilon_{\rm art}$ to the luminosity equation,

$$\frac{{\rm d}L}{{\rm d}m} = \epsilon_{\rm nuc} - T\frac{{\rm d}S}{{\rm d}t} + \epsilon_{\rm art}. \tag{4}$$

Here, $\epsilon_{\rm nuc}$ is the net energy generation rate from nuclear reactions, S is entropy per unit mass, T is the temperature and $-T{\rm d}S/{\rm d}t$ is the energy released by gravitational contraction. This term vanishes for stars in thermal equilibrium. As mentioned collision remnants are out of thermal equilibrium and the effect of $\epsilon_{\rm art}$ is to specify $T{\rm d}S/{\rm d}t$. A suitable form is given by

$$-T\frac{{\rm d}S}{{\rm d}t} + \epsilon_{\rm art} = T\frac{\Delta S}{\tau}, \tag{5}$$

where ΔS is the difference in entropy between the current model and the target model and τ is an artificial timescale on which the adjustment is to be made. With this choice an equilibrium is reached when the entropy profile in the model matches that of the target model, $\Delta S = 0$. The timescale τ is arbitrary in principle and can be chosen to change the relative weight of the terms in the energy equation, which affects the speed of convergence. Choosing τ to be of the order of the current timestep was found to work well.

At the same time, the composition profile is changed smoothly by setting

$$X \rightarrow (1-\lambda)X + \lambda X_{\rm target}, \tag{6}$$

where λ is increased monotonically from 0 to 1 in the course of the run. Composition changes due to nuclear reactions and mixing processes were ignored. We continue this procedure until the entropy and composition profiles in the model match those of the collision product. The final model is then used as a starting model for the evolution of the merger remnant.

This implicit scheme is very stable and flexible, and deals well with small irregularities in the output. Figure 1 shows that the resulting entropy and composition profiles agree very well with the target profiles. Except for the entropy profile in the core the two curves overlap within the thickness of the lines shown. We have tested whether small deviations like these affect the long-term evolution of the collision product and have found that they are unimportant.

Detailed SPH calculations do not have sufficient resolution to resolve the outer parts of the envelope of the collision product and MMAS likewise does not have any real information about this region. This means that the structure of the outer envelope cannot be determined from these models. Sills et al. (1997) extrapolated the entropy profile and used the condition of hydrostatic equilibrium to reconstruct the outer layers. We have

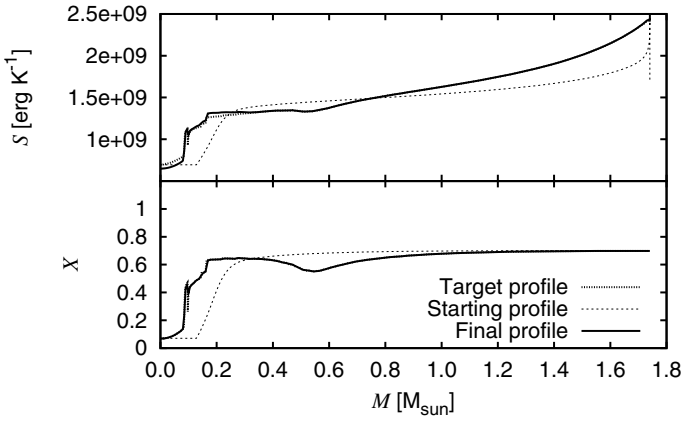

Fig. 1. Entropy (*top panel*) and hydrogen abundance (*lower panel*) profiles in the merger remnant 2321 (see Table 1) as a function of mass coordinate during the convergence stage. The profile at the start of the iteration is indicated by a thin dotted line while the target profile is indicated by a thick dotted line. The solid line is the final profile after the import is complete.

found it easier to assume that these layers are in thermal equilibrium and have not tried to impose a particular entropy profile in these layers. This is reasonable considering that the local thermal timescale is short compared to that of the rest of the star. Because we do not enforce a large entropy on the outer layers our models are somewhat less inflated than those of Sills et al. (1997) and consequently start at a lower luminosity. As pointed out by Sills et al. (1997) the long term evolution of the collision product is determined by the interior properties and is not sensitive to the assumptions made for the outer layers. Comparing their evolution tracks of collision products to tracks computed with our code for the same masses and metallicity confirms this. We find that the contraction timescales are similar and that the tracks agree from the main sequence onward.

In this work we ignore rotation in the collision products by assuming that all collisions are head-on. In the more realistic case of off-centre collisions the effect of rotation on the evolution of collision products can be substantial, as outlined in Sect. 1. We choose to ignore this problem for the moment and we defer a discussion of this limitation until Sect. 5.2.

2.4. The BSE/NBODY4 prescription

We will compare the outcome of our detailed evolution models with the results obtained in the *N*-body calculations of Hurley et al. (2005). These calculation were performed using the NBODY4 code Aarseth (1999) in which binary evolution is provided by the Binary Star Evolution (BSE) algorithm (Hurley et al. 2002). In this algorithm a simple analytic prescription is used to model the outcome of stellar collisions where no mass is lost during the collision, i.e. the remnant mass is $M_1 + M_2$. The merger remnant is replaced by a normal evolved main-sequence star with a starting age t' given by

$$t' = \frac{1}{10}\frac{\tau_{\rm ms}}{M_1+M_2}\left(M_1\frac{t}{\tau_{\rm ms,1}} + M_2\frac{t}{\tau_{\rm ms,2}}\right), \quad (7)$$

so that the remaining lifetime of the collision product is $t_{\rm ms,BSE} = \tau_{\rm ms} - t'$. Equation (7) is based on the implicit assumption that the remnant is fully mixed. Here $\tau_{\rm ms,1}$, $\tau_{\rm ms,1}$ and $\tau_{\rm ms}$ are the main-sequence lifetimes of the two colliding stars and of a normal star with mass $M_1 + M_2$, respectively. These lifetimes are calculated according to the analytic formulae of Hurley et al. (2000) which are based on detailed models that include convective overshooting (Pols et al. 1998).

3. Evolution of the merger remnants

The masses M_1 and M_2 of the colliding stars and the time of collision t are taken from the *N*-body simulation of M 67 by Hurley et al. (2005) and are listed in Table 1. The collisions listed as 3289-2 and 3835-2 are further collisions between a collision product and another main sequence star. In the case of 3289-2 this results in a collision product that is more than twice as massive as the most massive progenitor star. The most massive collision product in our list, however, is 2203.

We have constructed starting models for the calculation of the evolution of the collision products in Table 1 using the method described in Sect. 2. All models are calculated for an initial hydrogen mass fraction $X = 0.70$ and a mass fraction of heavy elements $Z = 0.02$. For the double collisions 3289 and 3835 we have used the output of the first collision as input for the second collision. All collision products were then allowed to evolve until the tip of the giant branch.

For each evolution model based on the MMAS output we have calculated two evolution tracks for comparison. One is a star with the same mass as the collision product that is evolved from the ZAMS at composition $X = 0.70$ and $Z = 0.02$, the other is a homogenised version of the collision product.

Table 1 also lists the total remnant mass M according to MMAS, the remaining main-sequence lifetime $t_{\rm ms}$ according to our detailed evolution models, the main-sequence lifetime $\tau_{\rm ms}$ of a star with the same ZAMS mass and the lifetime of a homogenised version of the collision product, $\tau_{\rm ms,hom}$. The lifetimes listed for 3289-1 and 3835-1 are the lifetimes these merger remnants would have had if they had not been involved in a second collision. Also given in Table 1 is the remaining lifetime according to the BSE prescription, $t_{\rm ms,BSE}$ (see Sect. 4 for a comparison and discussion).

In Fig. 2 we have plotted the evolution tracks of our models in the Hertzsprung-Russell diagram. The solid lines are the evolution tracks of the detailed collision products while the dotted lines are the evolution tracks of the normal stars. The homogenised models are indicated by a dashed line. We see that in general, the homogenised models are hotter and brighter than the normal models, while the collision products tend to be brighter than the normal stars but less luminous than the homogenised models. This is an opacity effect, as will be discussed below.

3.1. Initial structure and contraction phase

Initially, all collision products have a large amount of excess thermal energy and the star's main energy source is gravitational contraction. We refer to this initial phase where the collision product is puffed up and out of thermal equilibrium as the contraction phase.

There is no significant mixing during the collision. This can lead to composition inversions in the remnant: the core is rich in helium, on top of which there is a hydrogen-rich layer above which there is again a helium-rich layer of material from the core of the primary. These composition inversions show up in models where the primary star is sufficiently evolved to have burned a significant fraction of its central hydrogen to helium while the secondary is relatively unevolved, i.e. where the secondary is much less massive than the primary. Consequently, they are present in models 2203, 2321 and 3121 as well as the

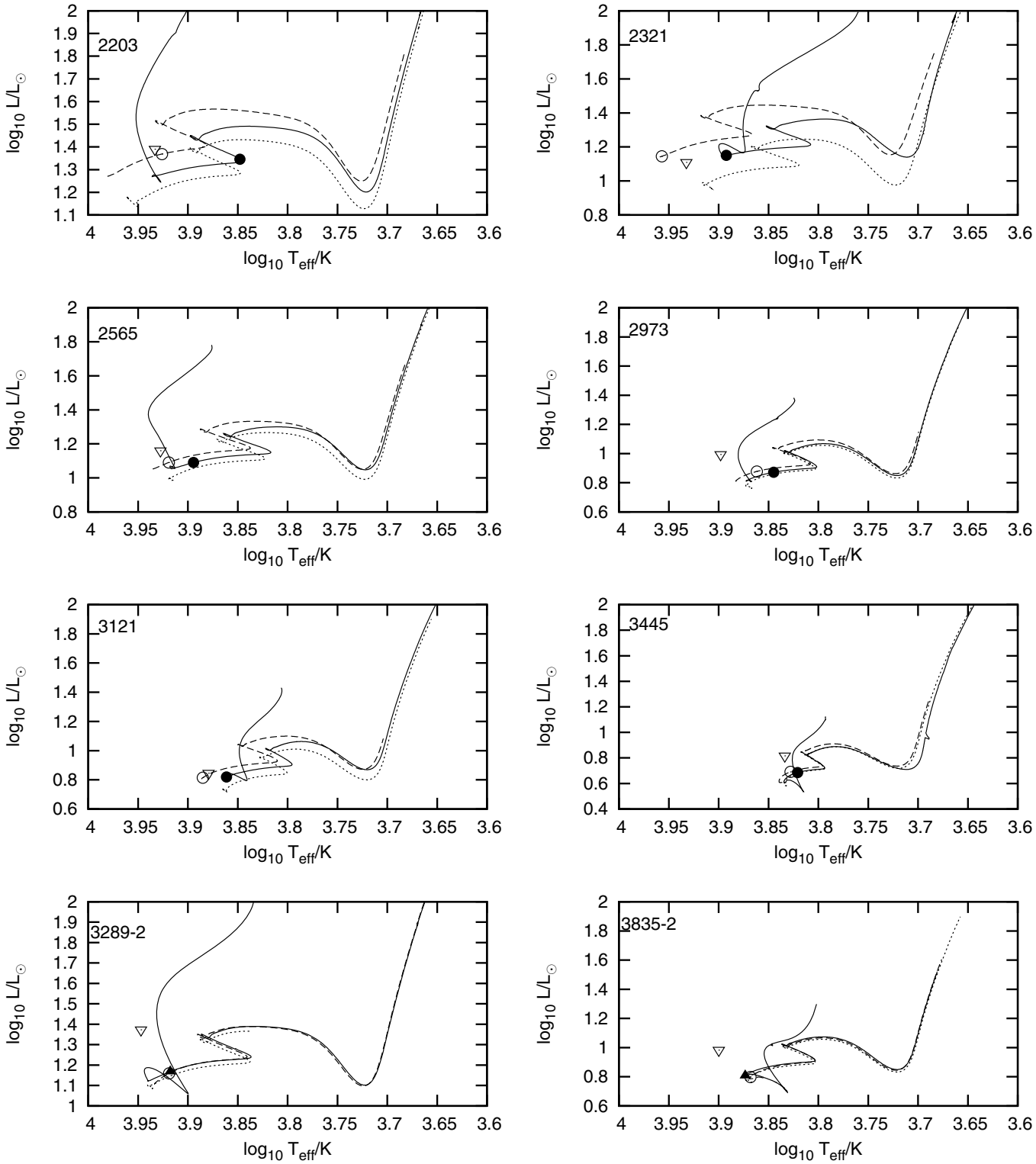

Fig. 2. Evolution tracks for the collision products (solid lines) compared to tracks for homogenised models (dashed lines) and a main sequence star of the same ZAMS mass (dotted line). Also marked are the positions at 4 Gyr for the detailed models (• for remnants of a single collision and ▲ for the remnants of two collisions), the homogenised models (⊙) and the BSE prescription (▽).

two double mergers 3289 and 3835, although the composition inversions are small in this case. As mentioned in Sect. 2.2, a composition inversion of this type is secularly unstable and leads to thermohaline mixing. This homogenises part of the central region of the remnant.

As an illustrative example, we will discuss in more detail the various evolutionary stages of the collision product 2321. This exhibits many of the transient features that occur during the evolution of these collision products.

First we consider the composition profile for collision 2321 which is shown in Fig. 3. During the collision a large portion of the core of the 1.29 $M_\odot$ primary has sunk to the centre, creating a hydrogen poor core below mass coordinate 0.1 $M_\odot$. Above this region material is slightly mixed with material from the

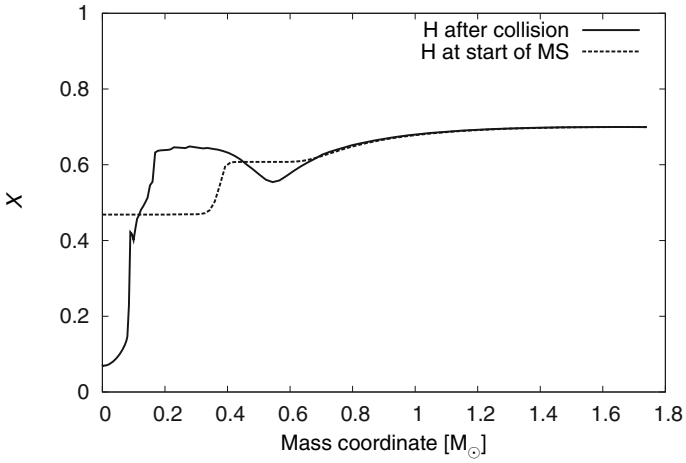

Fig. 3. Composition profiles in the merger remnant 2321, immediately after the collision (solid line) and on reaching the main sequence (dashed line).

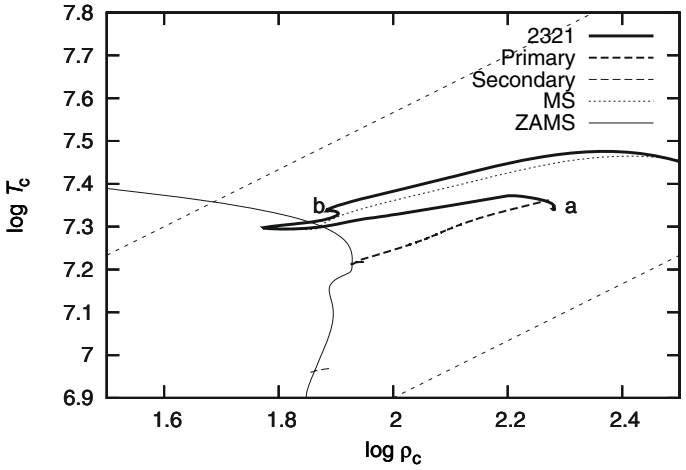

Fig. 4. Evolution track for the collision product 2321 in a ρ_c–T_c diagram (thick solid line). Also plotted are the progenitor tracks (dashed lines), the track for a star with the same ZAMS mass as the collision product (dotted line) and the location of the ZAMS (thin solid line). The short-dashed lines represent lines of constant entropy for a given composition. The collision product starts with an overdense core at the point labeled *a* and reaches the main sequence at point *b*.

0.59 $M_\odot$ secondary, leading to a hydrogen-rich layer between 0.2 and 0.4 $M_\odot$. On top of this there is a helium-rich layer at mass coordinate 0.6 $M_\odot$. Between this layer and the surface of the star the composition tends to the primordial composition.

The helium-rich layer at 0.6 $M_\odot$ is unstable to thermohaline mixing, which will mix the helium inward while the star contracts to the main sequence. At the same time, hydrogen will reignite in a shell at 0.1 $M_\odot$. This burning shell forms as a result of a peak in the hydrogen burning rate due to the steep increase of the hydrogen abundance in this region. The shell drives a convection zone that connects to the thermohaline layer and mixes the inner 0.4 $M_\odot$ of the star. This mixes helium-rich material into this burning shell which has the effect of lowering its efficiency. By the time the merger remnant has reached the main sequence the burning shell has extinguished. We define the endpoint of the contraction phase as the moment where central hydrogen burning takes over as the main energy source and the star is in thermal equilibrium.

At this point the central hydrogen abundance has increased to a mass fraction of 0.46 and the composition profile has changed to the dashed line in Fig. 3. The collision product has a convective core on the main sequence that extends to about 0.2 $M_\odot$.

The evolution of the core is shown in Fig. 4, where the central temperature T_c is plotted against the central density ρ_c. The short-dashed lines indicate lines of constant entropy with entropy increasing in the direction of increasing temperature and decreasing density. The core starts at point *a* with an entropy that is close to that of the core of the former primary. This means that the core has an entropy that is too low for a star of its mass and it will need to increase its entropy before the star can come into thermal equilibrium. This increase in entropy is achieved by expansion, which means that the core moves to the left in the diagram until it reaches the correct adiabat. At this point the core starts to contract again until thermal equilibrium is finally reached at point *b*. At this point the core is slightly hotter than the core of a star that was born with the same ZAMS mass.

3.2. Main sequence evolution

After the contraction phase the collision products follow more or less normal main-sequence tracks, although their luminosity (Fig. 2) and central temperature (Fig. 4) are typically higher than they would have been for a main sequence star of the same ZAMS mass. This is owing to the helium enhancement in their envelopes, which increases the mean molecular weight μ. The luminosity $L_{\rm merger}$ of the collision product scales with the luminosity of a normal star according to the homology relation (Kippenhahn & Weigert 1990)

$$L_{\rm merger} \approx L_{\rm ms} \left(\frac{\mu_{\rm merger}}{\mu_{\rm ms}} \right)^4 , \tag{8}$$

with $\mu_{\rm merger}$ and $\mu_{\rm ms}$ the mass-averaged mean molecular weight in the collision product and the main sequence star when these have the same effective temperature. The homology relation (8) is strictly valid only for homogeneous stars with constant opacity but it reproduces the luminosity shift of the merger remnants with respect to normal main sequence stars very well.

The higher effective temperature of the homogenised models results from a reduction of the average opacity owing to the increased helium content of their envelopes. The opacity affects the stellar structure by increasing or decreasing the photon mean free path. In the weakly mixed collision products, most of the helium enhancement is in the compact interior while the more extended envelope has the normal ZAMS composition. Thus, throughout most of the volume of the star a photon will "see" a normal hydrogen rich composition and the opacity is not strongly affected. Conversely, in the homogenised models the helium enhancement is present in the entire envelope and a photon will "see" a helium-enhanced composition with a lower opacity, leading to a more compact structure.

Because the luminosity is enhanced the collision products do not lie exactly on the extension of the main sequence, but can lie somewhat above it. As a consequence of their higher luminosity, the central temperature of the collision products is slightly increased (see Fig. 4) and the main-sequence lifetime (i.e. the time until core hydrogen exhaustion) is reduced compared to the lifetime of a normal main sequence star with a similar composition in the core.

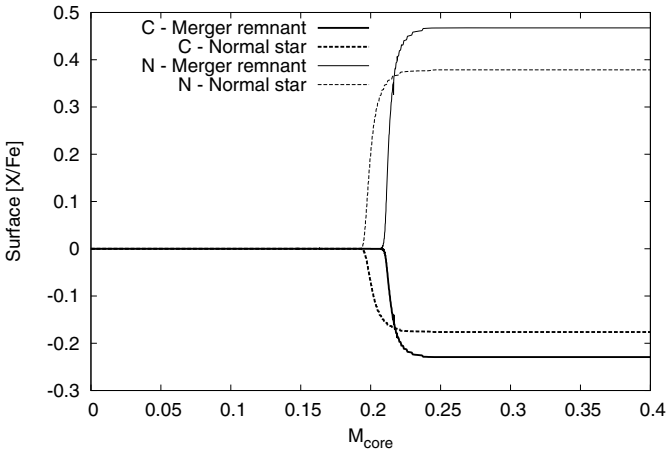

Fig. 5. Surface [C/Fe] and [N/Fe] abundances as a function of the helium core mass (as a measure of age) for collision product 2321. The carbon abundance (thick solid line) in the collision product is depleted when compared to a normal red giant (thick dashed line) while the nitrogen abundance (thin lines) is correspondingly enhanced.

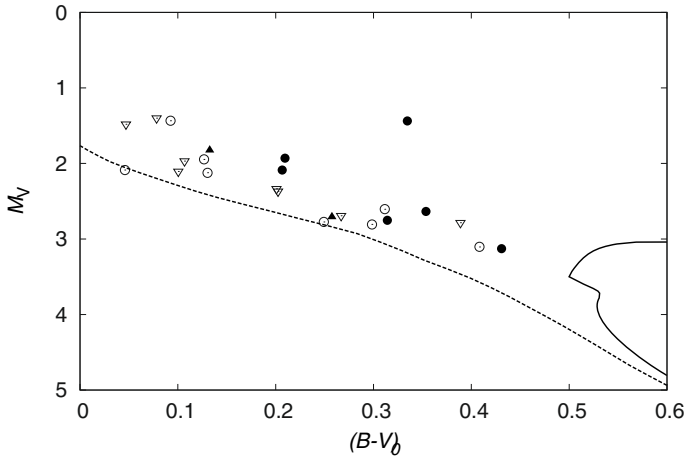

Fig. 6. Location in the colour-magnitude diagram of the blue stragglers at 4Gyr. Detailed models of the single collision remnants are indicated by • and double collision remnants by ▲. Homogenised models are indicated by ⊙ and the BSE prescription is indicated by ▽. The isochrones for $t = 0$ and $t = 4$ Gyr are constructed from the models by Pols et al. (1998).

3.3. Hertzsprung gap and first giant branch

We follow the evolution of the collision products through the Hertzsprung gap up to the tip of the giant branch. We were unable to calculate models beyond the helium flash.

The red giant phase is very similar to that of a normal star. The first dredge-up occurs when the convective envelope penetrates into the helium-rich layer. For our example collision product 2321 this increases the surface helium abundance to $Y_s = 0.334$ compared to $Y_s = 0.296$ in a normal red giant of the same mass. More of the dredged-up material has undergone processing than in a normal red giant because part of this material comes from the core of the original primary. As a result, more carbon has been converted to nitrogen by CN cycling, which enhances the nitrogen abundance and depletes the carbon abundance compared to a normal red giant, both by ∼0.1 dex in the case of collision 2321 as shown in Fig. 5. Unfortunately this does not exceed the typical observational error bar of 0.15 dex (for instance Gratton et al. 2000).

3.4. Double collisions

In the *N*-body simulation two blue stragglers are present at $t = 4$ Gyr that resulted from consecutive collisions between three stars in a binary-binary interaction. In both cases the second collision happened almost immediately after the first. We have not considered the situation where the time between collisions is long enough for the collision product to have evolved before the second collision. We have calculated the outcome of the first collision and used that as input for the second collision. These double collision remnants evolved in a similar way to single collision products and their main sequence evolution is very similar to that of ordinary stars of their mass. This can be understood from the fact that their progenitors are all fairly low-mass stars that are essentially unevolved at the time of collision. For this reason collision product 3289-2 has the highest effective temperature (Fig. 2) and the bluest colour (see Fig. 6 in Sect. 4), even though it is not the most massive collision product. It is likely that the structure and evolution of double collisions involving more massive and thus more evolved stars, or with more time passing between the collisions, will produce remnants that stand out more. The bluest blue straggler in M 67 (S977; Mathys 1991) is quite possibly the result of a double collision.

4. Comparison of different methods

In Fig. 2 we show as solid symbols the locations in the Hertzsprung-Russell diagram of each of the merger products listed in Table 1 after 4 Gyr (the age of M 67 obtained by isochrone fitting in Pols et al. 1998) and compare these to the locations of the homogenised models (open symbols) and the positions according to the BSE prescription (triangles). In Fig. 6 we show the corresponding locations for all collision products in a colour-magnitude diagram. A comparison between the observed blue stragglers and our models is given in Paper II. We converted the theoretical surface parameters (L, $T_{\rm eff}$ and $\log g$) to observable magnitude and colour (M_V, $B - V$) using model atmospheres from Kurucz (1992) with empirical corrections from Lejeune et al. (1997). Also shown is the location of the ZAMS (dashed line) and the $t = 4$ Gyr isochrone from Pols et al. (1998). The detailed models are redder than the homogenised models and the positions predicted by the BSE recipe, with the largest difference occurring for the brightest and most massive blue stragglers.

The homogeneous models are bluer than the detailed models for two reasons. First, the helium abundance in the envelopes of the homogeneous models is enhanced over that of the detailed models, which moves the position of the ZAMS line to the blue. Second, if we compare the lifetimes listed in Table 1 we see that the remaining lifetime for the homogenised models is longer than that of the detailed models, so that the homogenised models are closer to their zero-age main sequence. This is particulary striking in remnant 2203 (Fig. 2), for which the detailed model has almost reached the terminal-age main sequence point. The longer lifetime of the fully mixed models is due to the larger hydrogen abundance in their cores compared to the detailed models. The largest discrepancy is found for progenitor stars that were substantially evolved at the time of collision, in particular remnant 2321. The best match between detailed and fully mixed models is obtained for the double collision remnants, whose progenitor stars were not very evolved. In general the approximation

of homogeneous mixing is worse for collisions involving more evolved stars than for collisions involving less evolved stars.

The BSE recipe gives locations that are brighter and bluer mainly because mass loss from the collision is not considered, leading to higher remnant masses. As can be seen from Fig. 2 this effect is most noticeable in remnants 2973 and 3445 and the two double collision remnants 3289-2 and 3835-2. Because BSE simply uses a normal main-sequence star model for the collision remnant, the effect of the higher mass on the luminosity is at least partially compensated by neglecting the effect of helium enhancement.

The BSE prescription assumes complete mixing to estimate the remaining lifetime of the merger remnant. The BSE lifetimes are generally longer than those of both our detailed models (by more than a factor 2 in the case of remnant 2321) and the fully mixed models, despite the fact that the overestimate of the remnant mass by BSE would result in an underestimate of the lifetime by 20–30 per cent. This is, however, counteracted by two effects when compared to our fully mixed models. First, the neglect of helium enhancement leads to an increase of the lifetime by up to 30 per cent for collision remnants of evolved progenitor stars. Second, the inclusion of convective overshooting in the BSE models gives rise to longer main-sequence lifetimes, by 25–30 per cent in the mass range considered (see Sect. 5.2 for a discussion of this issue). A fairer comparison of the BSE *method* is to compute the remnant lifetime using Eq. (7) but inserting main-sequence lifetimes of non-overshooting models; we then find BSE lifetimes that are indeed somewhat smaller than those of our fully mixed models.

The homogeneous models and the BSE prescription can both produce blue stragglers that are brighter and bluer than those produced by the detailed models. In the case of the BSE models this is due to the higher mass of the collision products, while in the case of the homogeneous models this is due to the higher helium content of their envelopes. This implies that in order to form the brightest blue stragglers it may be necessary to collide more massive progenitor stars, or that enhanced mixing in the collision products (for instance due to rotation) is necessary.

5. Discussion

5.1. Convective overshooting

There is evidence that for ordinary stars in the mass range we consider mixing extends beyond the boundary of the classical convective core, which is usually modelled by convective overshooting as discussed in Schröder et al. (1997). As mentioned in Sect. 2.2, we have disabled convective overshooting for the evolution of the merger remnants. During the contraction phase in some of the remnants, regions develop where $\nabla_{\rm rad} - \nabla_{\rm ad}$ is close to zero but remains negative ($\nabla_{\rm rad} - \nabla_{\rm ad} > -\delta$), so that these regions never actually become convective. The overshooting prescription used in our code leads to undesired spurious mixing in such regions.

Convective overshooting affects the lifetime and the shape of the main-sequence track of a star. The progenitor stars will mostly not be overly affected by overshooting (because their masses are too small to develop convective cores), whereas the collision product is massive enough to experience overshooting. The main difference we expect is that for two given parent stars the collision product will have a larger reservoir of hydrogen and live longer. The inclusion of overshooting in our detailed models would likely make the collision remnants of evolved parent stars (such as 2203) somewhat bluer, because the enhanced mixing brings the remnant closer to its ZAMS position. More importantly, the lifetimes of all our collision products would be increased, perhaps by about 30 per cent (based on comparing overhooting and non-overshooting models from Pols et al. 1998).

5.2. Rotation

We have ignored rotation in the present work by treating all collisions as head-on. Rotation will modify our results by extra mixing and possibly by enhanced mass loss. The latter is particularly relevant because off-centre collisions produce remnants that have so much angular momentum that their rotation rate will approach critical rotation during the contraction phase. How the remnant loses angular momentum is still an unsolved problem and it is likely that magnetic fields play a role here, possibly by coupling the star to a circumstellar disk (Sills et al. 2005). At present, nothing is known about the magnetic field in the collision product after the collision.

Rotational mixing provides a larger hydrogen reservoir for nuclear burning and increases the helium content in the envelope, making the remnants bluer and brighter and extending their lifetimes (Sills et al. 2001). By ignoring rotation we implicitly assume that an efficient spin-down mechanism operates in the collision products such that they avoid both the angular momentum problem and significant rotational mixing. It is significant that the blue stragglers in M 67 are slow rotators, with projected rotation velocities smaller than typical for their spectral type (Peterson et al. 1984; Mathys 1991). Since all formation mechanisms for blue stragglers are expected to result in rapid rotation, this suggests that they can indeed lose angular momentum efficiently. We will investigate this problem in more detail in future work.

6. Conclusions

Hydrodynamical simulations of stellar collisions produce remnants that are out of thermal equilibrium and are not fully mixed. We have developed an efficient procedure for importing the structural and chemical profiles of such collision products into a fully implicit stellar evolution code. Our evolution code is fairly robust and can evolve the collision remnants until the tip of the giant branch with a minimum of human intervention. We have applied our code to construct detailed models of collisional blue stragglers formed in the *N*-body simulation of M 67 by Hurley et al. (2005).

The evolution of collision products depends on the amount of mixing during the collision and the thermal relaxation phase. Assuming the collision product has been homogeneously mixed produces evolution tracks that are too blue while replacing the collision product with a normal star of the same mass (as done in the simulations of Hurley et al. 2005) produces an evolution track that is not bright enough. Both approximations overestimate the lifetime of the collision product. These considerations will affect the predicted colour–magnitude diagram distribution of collisional blue stragglers from a cluster simulation.

Our code is suitable for a systematic exploration of the wide parameter space of collisions in clusters of different ages. This will be the topic of future papers. Eventually we hope to integrate our code into a full *N*-body code to allow for more realistic and self-consistent star cluster simulations.

Acknowledgements. We thank the referee, Alison Sills, for useful comments that improved this paper. E.G. acknowledges support from NWO under grant 614.000.303

Appendix A: Modifications to the evolution code

It is a feature of the STARS code that it solves the stellar structure equations simultaneously with the reaction-diffusion equations for the different abundances on a moving mesh. The code is normally fast and reliable, but we have found that it sometimes has difficulty evolving our merger remnants and have come up with a scheme that helps it evolve through "difficult" timesteps.

Consider the set of independent variables $\boldsymbol{H}$ that represents a solution to the stellar structure equations at time t. The problem is then to find the changes $\Delta\boldsymbol{H}$ such that $\boldsymbol{H} + \Delta\boldsymbol{H}$ represents the solution at time $t + \Delta t$. An initial guess for ΔH can be taken from the previous timestep and then improved by iteration in a Henyey-like solver. If no solution can be found, a smaller timestep can be tried. In some cases, this leads to a runaway situation where repeated convergence failures cause the timestep to drop until it drops below a threshold value and the code aborts.

The cause of the convergence failure is that the initial guess for the corrections $\Delta\boldsymbol{H}$ is not close enough to the desired corrections. We have looked for ways to improve the initial guess in case of convergence failure.

Often it is possible to identify the terms in the equations that cause difficulty. A common example are the diffusion terms in the reaction-diffusion equations,

$$\frac{\mathrm{d}X_i}{\mathrm{d}t} = -\frac{1}{\rho r^2}\nabla\rho r^2\sigma\nabla X_i + R_i, \tag{A.1}$$

where X_i represents the abundance of species i, σ is the sum of all diffusion coefficients affecting the composition and R_i is the production (or destruction) rate of species i due to nuclear reactions. In case of convergence problems, it can help te eliminate or reduce ("relax") the diffusion coefficient σ. The resulting corrections $\Delta\boldsymbol{H}'$ are not the final corrections, but they might be a better first guess than the values used previously.

Convective mixing is the most common example where our above relaxation scheme is useful, but it is by no means the only one. Other examples where we have found it useful in our code are the nuclear energy generation rate (which is then relaxed from the value at the previous timestep), the mass loss rate and advection terms in the luminosity equation.

References

Aarseth, S. J. 1999, PASP, 111, 1333
Ahumada, J., & Lapasset, E. 1995, A&AS, 109, 375
Alexander, D. R., & Ferguson, J. W. 1994, ApJ, 437, 879
Anders, E., & Grevesse, N. 1989, Geochim. Cosmochim. Acta, 53, 197
Bailyn, C. D., & Pinsonneault, M. H. 1995, ApJ, 439, 705
Böhm-Vitense, E. 1958, ZsAp, 46, 108
Caughlan, G. R., & Fowler, W. A. 1988, Atomic Data and Nuclear Data Tables, 40, 283
Caughlan, G. R., Fowler, W. A., Harris, M. J., & Zimmerman, B. A. 1985, Atomic Data and Nuclear Data Tables, 32, 197
Eggleton, P. P. 1971, MNRAS, 151, 351
Eggleton, P. P. 1972, MNRAS, 156, 361
Glebbeek, E., & Pols, O. R. 2008, A&A, 488, 1017
Gratton, R. G., Sneden, C., Carretta, E., & Bragaglia, A. 2000, A&A, 354, 169
Hills, J. G., & Day, C. A. 1976, ApJ, 17, L87
Hurley, J. R., Pols, O. R., & Tout, C. A. 2000, MNRAS, 315, 543
Hurley, J. R., Tout, C. A., Aarseth, S. J., & Pols, O. R. 2001, MNRAS, 323, 630
Hurley, J. R., Tout, C. A., & Pols, O. R. 2002, MNRAS, 329, 897
Hurley, J. R., Pols, O. R., Aarseth, S. J., & Tout, C. A. 2005, MNRAS, 363, 293
Johnson, H. L., & Sandage, A. R. 1955, ApJ, 121, 616
Kippenhahn, R., & Weigert, A. 1990, Stellar Structure and Evolution, XVI, 468 (Berlin Heidelberg New York: Springer-Verlag), Also Astronomy and Astrophysics Library
Kippenhahn, R., Ruschenplatt, G., & Thomas, H.-C. 1980, A&A, 91, 175
Kurucz, R. L. 1992, in The Stellar Populations of Galaxies, ed. B. Barbuy, & A. Renzini, IAU Symp., 149, 225
Landau, L. D., & Lifshitz, E. M. 1980, Statistical physics. Pt.1, Pt.2, Course of theoretical physics, Pergamon International Library of Science, Technology, Engineering and Social Studies (Oxford: Pergamon Press), 3rd rev. and enlarg. edn.
Lejeune, T., Cuisinier, F., & Buser, R. 1997, A&AS, 125, 229
Lombardi, Jr., J. C., Rasio, F. A., & Shapiro, S. L. 1995, ApJ, 445, L117
Lombardi, Jr., J. C., Rasio, F. A., & Shapiro, S. L. 1996, ApJ, 468, 797
Lombardi, Jr., J. C., Warren, J. S., Rasio, F. A., Sills, A., & Warren, A. R. 2002, ApJ, 568, 939
Mathys, G. 1991, A&A, 245, 467
Peterson, R. C., Carney, B. W., & Latham, D. W. 1984, ApJ, 279, 237
Pols, O. R., Tout, C. A., Eggleton, P. P., & Han, Z. 1995, MNRAS, 274, 964
Pols, O. R., Schroder, K.-P., Hurley, J. R., Tout, C. A., & Eggleton, P. P. 1998, MNRAS, 298, 525
Rogers, F. J., & Iglesias, C. A. 1992, ApJS, 79, 507
Sandage, A. R. 1953, AJ, 58, 61
Sandquist, E. L., Bolte, M., & Hernquist, L. 1997, ApJ, 477, 335
Schröder, K.-P., Pols, O. R., & Eggleton, P. P. 1997, MNRAS, 285, 696
Sills, A., Bailyn, C. D., & Demarque, P. 1995, ApJ, 455, L163
Sills, A., Lombardi, Jr., J. C., Bailyn, C. D., et al. 1997, ApJ, 487, 290
Sills, A., Faber, J. A., Lombardi, Jr., J. C., Rasio, F. A., & Warren, A. R. 2001, ApJ, 548, 323
Sills, A., Adams, T., Davies, M. B., & Bate, M. R. 2002, MNRAS, 332, 49
Sills, A., Adams, T., & Davies, M. B. 2005, MNRAS, 358, 716
Stancliffe, R. J., Glebbeek, E., Izzard, R. G., & Pols, O. R. 2007, A&A, 464, L57
Stryker, L. L. 1993, PASP, 105, 1081
Tout, C. A., Aarseth, S. J., Pols, O. R., & Eggleton, P. P. 1997, MNRAS, 291, 732
Ulrich, R. K. 1972, ApJ, 172, 165